AB

SLAC-PUB-5606
January 1994
(E)

EVIDENCE FOR $\rho(1300)$ IN THE REACTION $K^-p \to \pi^+\pi^-\Lambda$ AT 11 GeV/c *

D. Aston,[1] N. Awaji,[2] T. Bienz,[1] F. Bird,[1] J. D'Amore,[3] W. Dunwoodie,[1] R. Endorf,[3] K. Fujii,[2] H. Hayashii,[2] S. Iwata,[2] W. Johnson,[1] R. Kajikawa,[2] P. Kunz,[1] Y. Kwon,[1] D. Leith,[1] L. Levinson,[1] J. Martinez,[3] T. Matsui,[2] B. Meadows,[3] A. Miyamoto,[2] M. Nussbaum,[3] H. Ozaki,[2] C. Pak,[2] B. Ratcliff,[1] P.E. Rensing,[1] D. Schultz,[1] S. Shapiro,[1] T. Shimomura,[2] P. Sinervo,[1] A. Sugiyama,[2] S. Suzuki,[2] G. Tarnopolsky,[1] T. Tauchi,[2] N. Toge,[1] K. Ukai,[4] A. Waite,[1] S. Williams[1]

[1]Stanford Linear Accelerator Center, Stanford University, Stanford, California 94309, USA
[2]Department of Physics, Nagoya University, Furo-cho, Chikusa-ku, Nagoya-shi 464, Japan
[3]Department of Physics, University of Cincinnati, Cincinnati, OH 45221, USA
[4]Institute for Nuclear Study, University of Tokyo, 3-2-1 Midori-cho, Tanashi-shi, Tokyo 188, Japan

Abstract

Results are presented from an analysis of the $\pi^+\pi^-$ system produced in the reaction $K^-p \to \pi^+\pi^-\Lambda$ at 11 GeV/c observed with the LASS Spectrometer at SLAC. A clear ρ–ω interference effect is observed, and a fit to the natural parity exchange mass distribution yields an estimate of $(1.5 \pm 0.5)\%$ for the branching fraction of the decay $\omega \to \pi^+\pi^-$. An amplitude analysis reveals that the bump in the mass distribution in the vicinity of the $f_2(1270)$ actually contains a significant P-wave component. The mass dependence of the corresponding amplitude and phase is well described by a resonant Breit–Wigner line shape with mass (1290^{+20}_{-30}) MeV/c^2, width (120^{+60}_{-50}) MeV/c^2, and small $\pi^+\pi^-$ elasticity. The interpretation of this state as the first radial excitation of the $\rho(770)$ is discussed. Evidence is presented for production of the $\rho_3(1690)$ in the $\pi^+\pi^-$ spectrum.

Submitted to Zeitschrift für Physik C

*Work supported in part by the Department of Energy under contract No. DE-AC03-76SF00515, the National Science Foundation under grant No. PHY92-04239, and the Japan U.S. Cooperative Research Project on High Energy Physics.

SLAC PUB 5606
SCN 9413

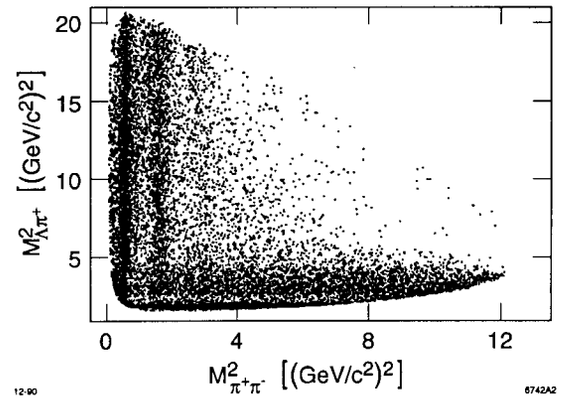

Fig. 1. The Dalitz plot for the events of reaction (1) with $-t_{p\to\Lambda} \leq 2(\mathrm{GeV/c})^2$.

1 Introduction

This paper presents results from an analysis of the $\pi^+\pi^-$ system observed in the reaction

$$K^-p \to \pi^+\pi^-\Lambda \qquad (1)$$

at an incident beam momentum of 11 GeV/c. Section 2 briefly discusses the data sample and characteristics of the final state, and Section 3 examines the ρ mass region and presents an analysis of the ρ–ω interference effect. Section 4 contains the results of an amplitude analysis pertaining to the P-wave of the forward $\pi^+\pi^-$ system produced by natural parity exchange. Section 5 discusses the high mass $\pi^+\pi^-$ spectrum while Section 6 gives results of the analysis of the backward $\pi^+\pi^-$ sample. Section 7 presents the cross sections measured in this analysis. Finally, Section 8 contains concluding remarks; the observed resonant state is discussed with respect to other experimental information, and also in the context of the quark model level structure. More details of the complete analysis can be found in [1].

2 The $\pi^+\pi^-\Lambda$ Final State

The data derive from an exposure of the Large Aperture Superconducting Solenoid (LASS) Spectrometer at SLAC to a K^- beam of 11 GeV/c. The spectrometer and relevant experimental details are described elsewhere [2]. The raw data sample contains $\sim$113 million triggers, corresponding to an integrated luminosity of 4.1 events/nb of useful beam flux. The acceptance is approximately uniform over almost the full 4π solid angle.

Four-constraint fits to events of the two-prong V^0 topology yield 32,371 events corresponding to reaction (1). Fig. 1 shows the Dalitz plot for events where the $\pi^+\pi^-$ system is

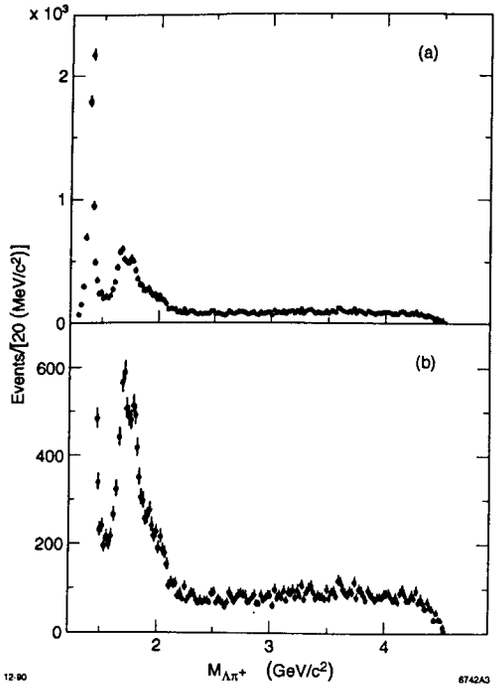

Fig. 2. The $\Lambda\pi^+$ mass projection for the forward $\pi^+\pi^-$ system (a) for all events and (b) with the $\Sigma(1385)$ region removed.

peripherally produced with respect to the incident K^- (*i.e.* forward in the center of mass frame); the selection criterion, $-t_{p\to\Lambda} \leq 2\,(\mathrm{GeV/c})^2$, results in a data sample consisting of 26,462 events. Clear resonance bands are observed for the $\pi^+\pi^-$ system in the vicinity of the $\rho(770)$ and $f_2(1270)$, and there is also an indication of a faint band near the $\rho_3(1690)$. Strong production of $\Sigma^+(1385)$ is observed in the $\Lambda\pi^+$ system (Fig. 2a), and there is clear evidence of the production of several higher mass Σ states in the mass range 1.6–2.1 $\mathrm{GeV/c^2}$ (Fig. 2b). No production of low-mass $\Lambda\pi^-$ states can be seen in Fig. 1; this is to be expected for slow Λ's, since the production of such states would require the exchange of a doubly-charged meson system in the t-channel. The Dalitz plot of Fig. 1 is very similar to those observed for reaction (1) at lower energies [3–6], demonstrating the uniformity of acceptance of the LASS spectrometer, trigger and software.

Fig. 3 shows the forward $\pi^+\pi^-$ mass distribution below $2\,\mathrm{GeV/c^2}$. The peak in the ρ region is severely distorted with respect to a single Breit–Wigner line shape; this is a consequence of ρ–ω interference, and will be discussed in the next section. There is a second

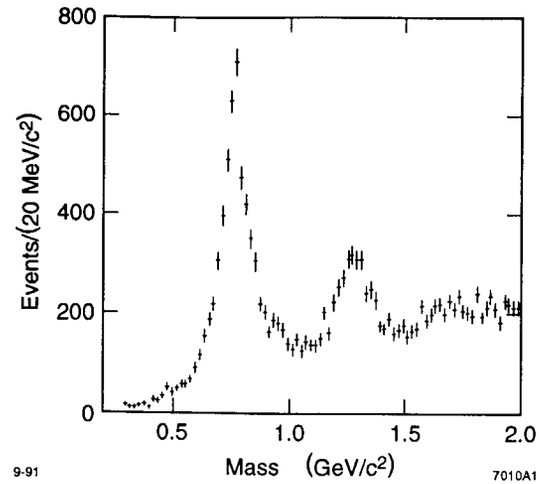

Fig. 3. The $\pi^+\pi^-$ mass projection corresponding to Fig. 1.

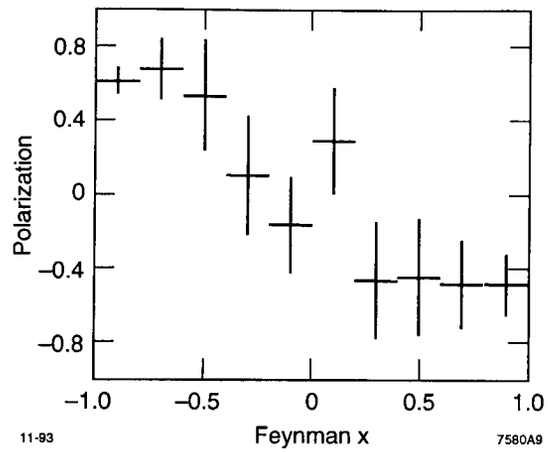

Fig. 4. The Λ polarization versus Feynman x of the Λ.

peak in the vicinity of the $f_2(1270)$; however, the analysis discussed in Section 4 shows that this is not due entirely to the production of this resonance. Finally, there is perhaps a small, broad enhancement at $\sim 1.7\,\mathrm{GeV/c^2}$; this would correspond to the faint band observed in Fig. 1, but it is hard to distinguish because it is small compared to the reflections of the Σ resonances.

The polarization of the Λ was measured from its decay asymmetry. The decay angle of the Λ was defined as the angle between the daughter proton and the decay plane normal, defined as $\hat{n} = (\hat{\Lambda} \times \hat{K})/|\hat{\Lambda} \times \hat{K}|$, where $\hat{K}$ and $\hat{\Lambda}$ are unit vectors along the incident beam and Λ momenta, respectively. Fig. 4 shows the polarization versus Feynman x, where the resonances in $\Lambda\pi^+$ below $2.1\,\mathrm{GeV/c^2}$ have been removed. The distribution is similar in shape to those measured at 4.2 GeV/c [4] and in inclusive lambda studies [7].

The observed events must be acceptance corrected in order to analyze the $\pi^+\pi^-$ system. This is accomplished by weighting each event by the inverse of the acceptance function (determined by Monte Carlo study) evaluated at the point in phase space corresponding to the event in question. Since the acceptance varies slowly, the resulting $\pi^+\pi^-$ mass spectrum is almost indistinguishable in shape from that of Fig. 3 (see t_{00} in Fig. 5); also, the t-channel spherical harmonic moments describing the $\pi^+\pi^-$ angular distribution,

$$t_{lm} = \sqrt{4\pi} \sum_{events} Y_l^m(\Omega), \tag{2}$$

exhibit the same structure before and after correction.

The next step in the analysis requires the removal of the overlap with Σ production. Events having a $\Lambda\pi^+$ mass between 1.3 and $1.52\,\mathrm{GeV/c^2}$ or between 1.6 and $2.15\,\mathrm{GeV/c^2}$ are removed from the data sample. The gap around $1.56\,\mathrm{GeV/c^2}$ is needed to keep the subsequent correction stable. Then, for each $\pi^+\pi^-$ mass bin, the t-channel moments are corrected, using the Monte Carlo sample, for the corresponding loss of real $\pi^+\pi^-$ events. The fully corrected moments for the forward $\pi^+\pi^-$ system are shown in Figs. 5, 6, and 7; moments with $m > 2$ or $l > 6$ are not needed to describe the data. The moments are computed for events with $t'_{p\to\Lambda} \leq 2.5\,(\mathrm{GeV/c})^2$. The steady drift away from zero at high mass in some of the moments, particularly those with $m = 0$, is a remnant of the Σ overlaps [1]; however, no more of the overlap can be removed without causing instabilities in the subsequent correction.

A partial wave analysis (PWA) was performed to estimate the resonance content of the data. First, the moments are expressed in terms of the underlying amplitudes describing the $\pi^+\pi^-$ system (see, for example, [8]). Spectroscopic notation is used to indicate the spin, with an additional subscript to indicate the type of t-channel exchange; a subscript of 0 denotes helicity 0, unnatural parity exchange, while subscripts of + and − indicate helicity 1, natural and unnatural parity exchange, respectively. A χ^2 minimization is used to extract the relevant amplitudes from the moments. It is important to include only the waves which are necessary to reproduce the moments, because unnecessary waves merely increase the uncertainties of the amplitudes. The highest spin wave included in the fit is determined by the structures seen in the moments; a spin L resonance can produce structure in the moments up to $l = 2L$. The fit is repeated many times with random starting parameters so that all acceptable solutions are found. More details can be found in [1].

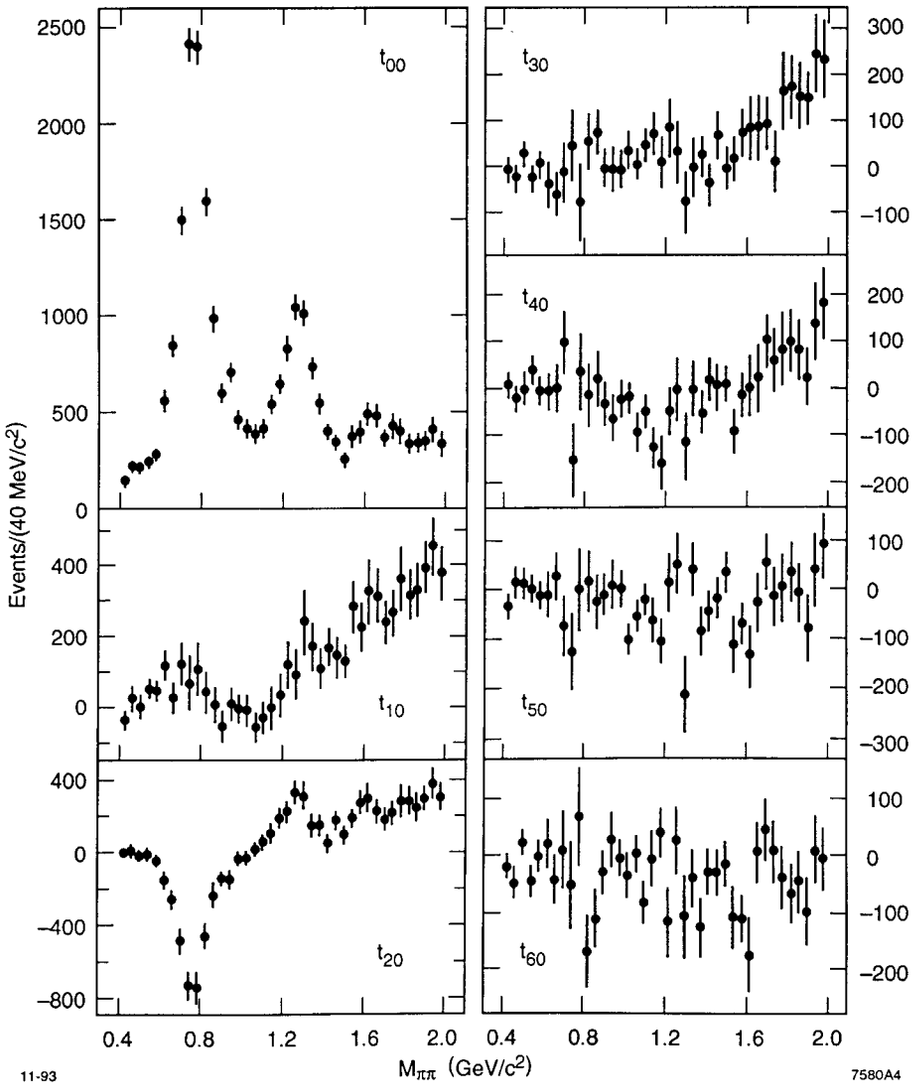

Fig. 5. The $m = 0$ acceptance corrected moments for the forward $\pi^+\pi^-$ system.

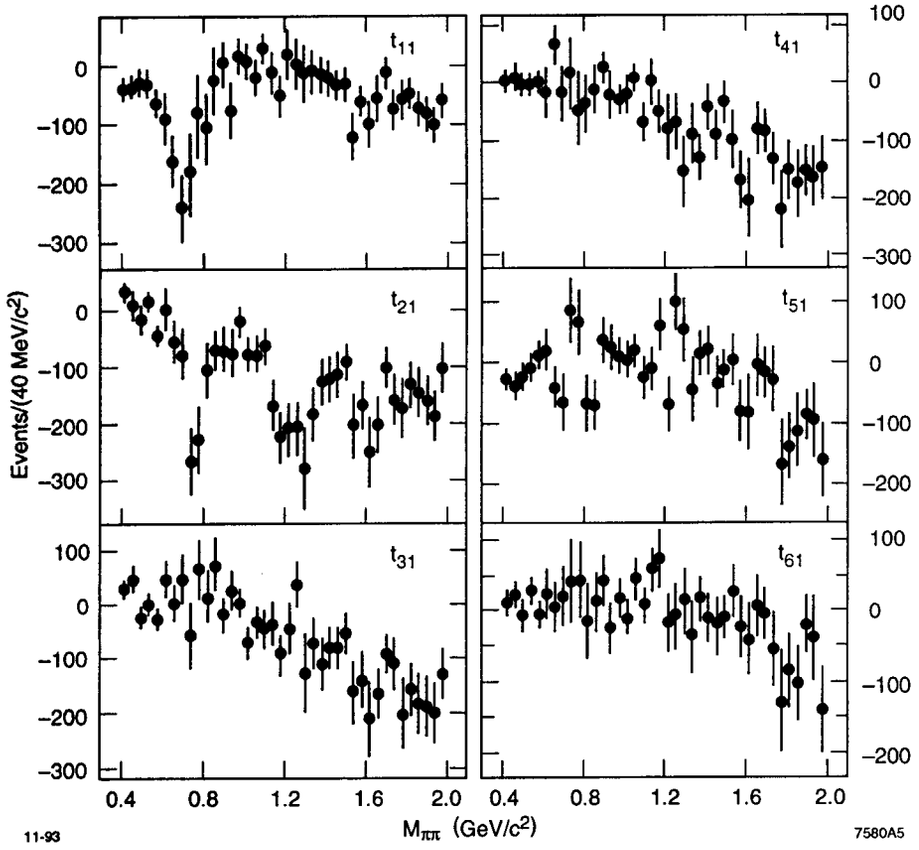

Fig. 6. The $m = 1$ acceptance corrected moments for the forward $\pi^+\pi^-$ system.

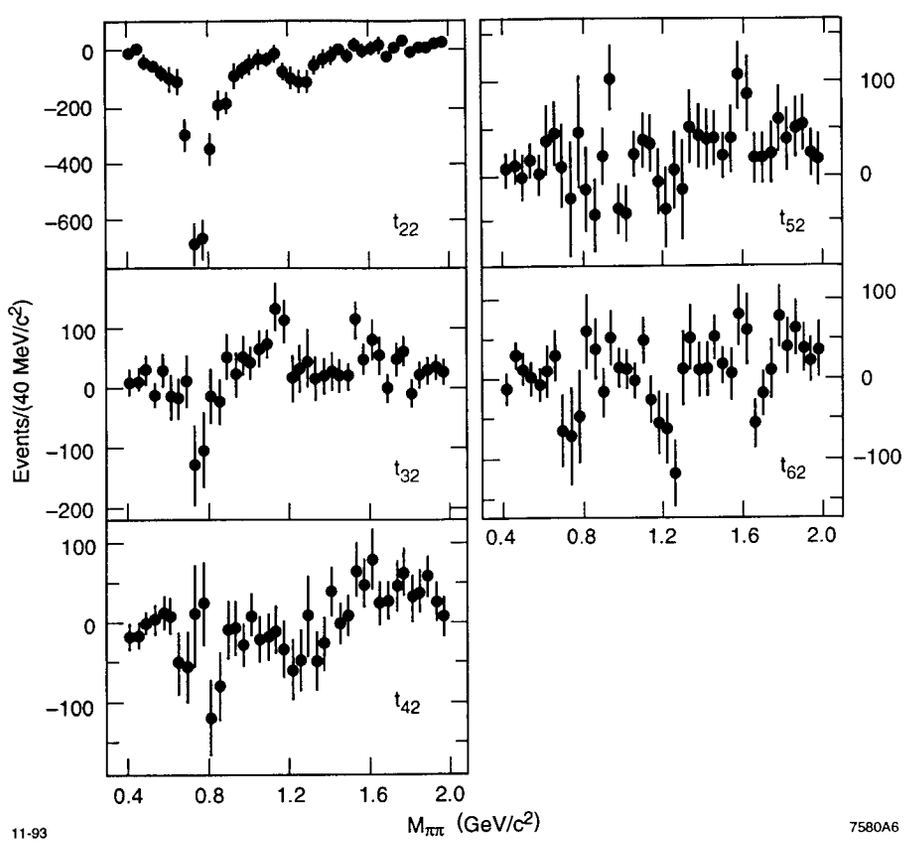

Fig. 7. The $m = 2$ acceptance corrected moments for the forward $\pi^+\pi^-$ system.

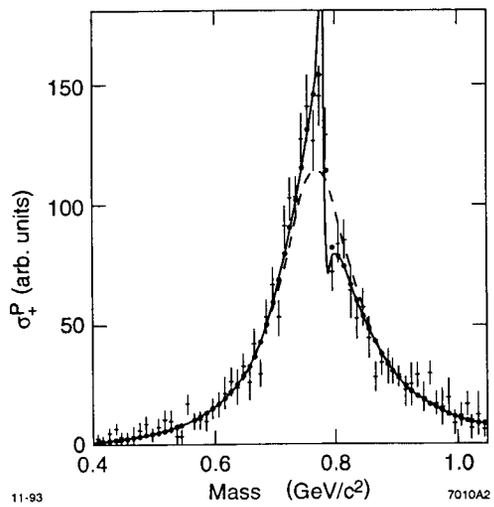

Fig. 8. The σ_+^P projection for the ρ ω interference region of Fig. 3. The data are shown as crosses, the solid curve represents the fit expression described in the text, and the dots correspond to the integral of this curve, after smearing for resolution, over each 10 MeV/c^2 bin. The dashed curve shows the contribution to the solid curve resulting from the ρ Breit–Wigner line shape.

3 Analysis of the ρ Region

For reaction (1), both the moments and the results of the partial wave analysis reveal that the $\pi^+\pi^-$ system is produced predominantly via natural parity (*i.e.* K*) exchange in the t-channel. In the ρ region, only S- and P-waves are required, and the combination of moments,

$$\begin{aligned} \sigma_+^P &\equiv \frac{1}{3}t_{00} - \frac{\sqrt{5}}{6}t_{22} \\ &= |P_+|^2 + |S|^2/3 \quad \text{(neglecting D-waves)}, \end{aligned} \tag{3}$$

which projects the P-wave natural parity exchange cross section, yields the mass distribution shown in Fig. 8. The S-wave contribution is negligible compared to that due to P_+.

The distribution of Fig. 8 cannot be described well by a single Breit–Wigner line shape (the dashed curve), and shows clear evidence of ρ–ω interference. Similar effects are observed for the corresponding, but much smaller, unnatural parity exchange cross sections; however, the associated uncertainties are larger, and so these will not be considered further here.

The possibility of significant ρ–ω mass mixing has been recognized for many years [9], and early estimates were that the resultant $\omega \to \pi^+\pi^-$ branching fraction might be 1–5% [9–11].

The direct transition element $T(\omega \to \pi^+\pi^-)$ has been calculated to be about 8 keV [12], and therefore can be neglected. If we define the relativistic propagator of particle x

$$P_x \equiv m_x^2 - m^2 - im_x\Gamma_x$$

and

$$\Delta \equiv \delta \cdot (m_\rho + m_\omega),$$

where δ is the complex mass-mixing term, then the ρ line shape, incorporating ρ–ω mixing to all orders, is given by

$$\frac{d\sigma}{dm} = \frac{d\sigma_\rho}{dm}\left|1 + \frac{A_\omega}{A_\rho}\frac{\Delta}{P_\omega}\right|^2 \left|1 - \frac{\Delta^2}{P_\rho P_\omega}\right|^{-2}, \tag{4}$$

where $d\sigma_\rho/dm$ is the ρ Breit–Wigner line shape, and A_ρ and A_ω are the ρ and ω production amplitudes, respectively [1]. The ρ Breit–Wigner is given by

$$\frac{d\sigma_\rho}{dm} = \frac{C\, m\Gamma(m)}{(m_\rho^2 - m^2)^2 + m_\rho^2\Gamma^2(m)}, \tag{5}$$

with C a constant, and

$$\Gamma(m) = \Gamma_0\left(\frac{q}{q_0}\right)^{2l+1}\left(\frac{m_0}{m}\right)\frac{D_l(q_0R)}{D_l(qR)}, \tag{6}$$

where the spin of the resonance, l, is 1 for the ρ, q is the momentum of one of the pions in the $\pi^+\pi^-$ rest frame, R is the range parameter ($R \sim 5\,\text{GeV}^{-1}$), D_l is a Blatt–Weisskopf polynomial [13], and the subscript 0 indicates a quantity evaluated at the resonance mass $m_0 = m_\rho$ or m_ω. The masses and widths of the ρ and ω were fixed to the Particle Data Group values [14] of $m_\rho = 768\,\text{MeV/c}^2$, $\Gamma_\rho = 151\,\text{MeV/c}^2$, $m_\omega = 782\,\text{MeV/c}^2$ and $\Gamma_\omega = 8.4\,\text{MeV/c}^2$. The fit yields $(2.15 \pm 0.35)\,\text{MeV/c}^2$ for the magnitude of the mass-mixing term, which implies a branching fraction of $(1.5 \pm 0.5)\%$ for the decay $\omega \to \pi^+\pi^-$, in reasonable agreement with the original estimates [9–11] and with the present world average of $(2.21 \pm 0.30)\%$ [14]. To obtain this number, complete coherence of the ρ and ω production amplitudes has been assumed; also, these production amplitudes have been assumed to be equal, as expected from SU(3). This is justified by the fact that the fitted value of the relative ρ–ω production phase is (-8 ± 10) degrees, consistent with the prediction by SU(3) of 0 degrees, and with data from other experiments [15]. The quality of the fit, as indicated by the solid dots in Fig. 8, is excellent, and the underlying line shape, represented by the solid curve, exhibits a rather spectacular interference effect.

Fitting the distribution in Fig. 8 with the resonance parameters free gives $(766 \pm 3)\,\text{MeV/c}^2$ for the mass, $(151 \pm 9)\,\text{MeV/c}^2$ for the width, and $5^{+3}_{-2}\,\text{GeV}^{-1}$ for the range parameter. The uncertainties are statistical only. This compares very well with the Particle Data Group's current world averages of $(768.1 \pm 0.5)\,\text{MeV/c}^2$, $(151.5 \pm 1.2)\,\text{MeV/c}^2$, and $5.3^{+0.9}_{-0.7}\,\text{GeV}^{-1}$ [14].

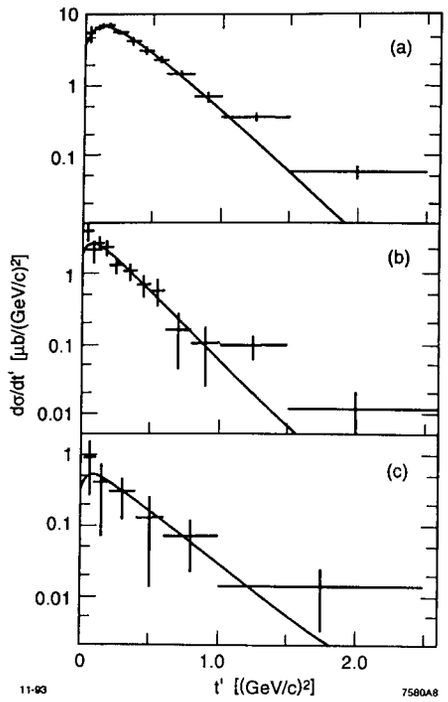

Fig. 9. The differential cross section for (a) σ_+^P, (b) σ_-^P, and (c) σ_0^P at the ρ. The curves represent the fits described in the text; only the points with $t' < 1.0\,(\mathrm{GeV/c})^2$ were fit.

Table 1. The results of fits of Eqn. (7) to the ρ differential cross sections.

Quantity	Exchange Mass m_{ex} (MeV/c^2)	Slope α ((GeV/c)$^{-2}$)	χ^2/DoF
σ_+^P	660 ± 110	3.1 ± 0.5	2.3 / 7
	890 (fixed)	3.90 ± 0.14	4.3 / 8
σ_-^P	440 ± 170	3.3 ± 1.4	4.1 / 8
	493 (fixed)	3.7 ± 0.6	4.2 / 8
σ_0^P	493 (fixed)	2.8 ± 1.7	0.5 / 3

Fig. 9 shows the differential cross sections, as a function of t', for the moments combinations σ_+^P, σ_-^P, and σ_0^P at the ρ. These plots were made by computing the moments *without* removing the Σ resonances. The background was removed by subtracting sidebands on either side of the ρ and renormalizing the number of events to the total cross section (see Section 7). The lowest bin extends down to $t' = 0.015\,(\mathrm{GeV/c})^2$ because the acceptance is too small to properly determine the cross section. The distributions for $t' < 1.0\,(\mathrm{GeV/c})^2$ were fitted with the form

$$\frac{d\sigma}{dt'} \propto \frac{[t' + (m_\Lambda - m_\mathrm{p})^2]\mathrm{e}^{-\alpha t'}}{(t' + m_{ex}^2)^2}, \tag{7}$$

where m_{ex} is the mass of the exchanged particle, namely the K* for natural parity exchange and the K for unnatural parity exchange. Two fits were performed, one in which the mass of the exchanged particle was allowed to vary and one in which it was fixed. Table 1 shows the results of the fits. The fitted exchange masses are roughly consistent with the expected values and all the fitted slopes are quite consistent with a single value of $\sim 3.8\,(\mathrm{GeV/c})^{-2}$.

4 Analysis of the $f_2(1270)$ Region

The amplitude analysis described in Section 2 was carried out for the $\pi^+\pi^-$ system using S- and P-waves (*i.e.* 6 parameters) in the mass region up to $1\,\mathrm{GeV/c^2}$ and S-, P- and D-waves (12 parameters) from 1 to $1.5\,\mathrm{GeV/c^2}$. The fit yield more than one solution to the PWA equations, and the amplitude values and their errors must reflect the presence of these multiple solutions. Each value is the average of any multiple solutions; the corresponding error is found by determining the points where the χ^2 function increases from its minimum by 4 (*i.e.* a 2σ interval) and dividing the distance by 2. If a 2σ point could not be found in the physical region, the 1σ point was used.

The S-wave found by the PWA is small and subject to large uncertainties. The ρ region is dominated by the P_+ amplitude, but P_- is also significant; P_0 is smaller than P_- and not very well defined. The D_+ and D_- waves show bumps at the $f_2(1270)$, but D_0 is essentially flat. An unexpected feature is that P_+, and to a lesser extent P_-, also exhibit structure in this mass range.

Figs. 10a, 10b, and 10c show the mass dependences of the P_+ and D_+ amplitudes and their relative phase, respectively. In the ρ region, the P_+ amplitude has the ρ–ω mixing structure discussed in Section 3; however, at higher mass, the amplitude does not simply decrease as the tail of the ρ Breit–Wigner (dotted curves), but shows a second maximum at $\sim 1.29\,\mathrm{GeV/c^2}$. The solid curves correspond to a simultaneous fit to the three quantities; in this fit, P_+ is described by the sum of the ρ–ω mixing amplitude and a Breit–Wigner describing the $1.29\,\mathrm{GeV/c^2}$ region, while the D_+ wave is represented by an $f_2(1270)$ Breit–Wigner. When dealing with amplitudes, a Breit–Wigner of spin l is given by

$$\frac{\sqrt{\Gamma(m)}}{m_0^2 - m^2 - im_0\Gamma(m)}, \tag{8}$$

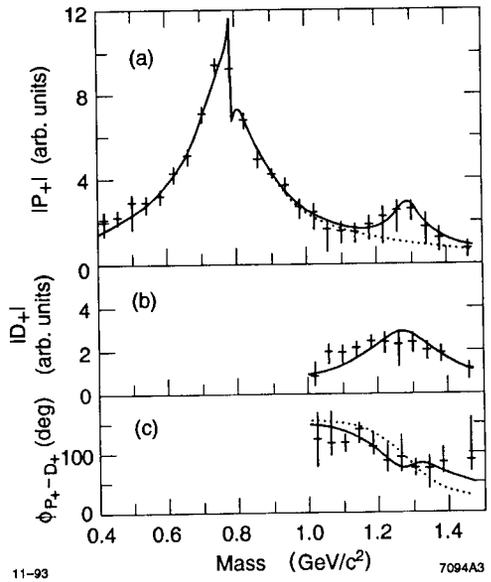

Fig. 10. The mass dependence of (a) the P_+ amplitude, (b) D_+ amplitude, and (c) P_+–D_+ relative phase resulting from the fits to the spherical harmonic moments described in the text. The solid curves represent a fit to the data allowing for a contribution from a P-wave Breit–Wigner around 1.29 GeV/c^2. The dotted curves correspond to the solid curves with the additional Breit–Wigner contribution set to zero.

with the width, $\Gamma(m)$, given by Eqn. (6). The range parameter R was fixed to 5 GeV^{-1} for all the resonances. The fit results are shown in Table 2 as "Fit A". A fit to the data excluding the second P-wave resonance, shown as the dotted curves in Fig. 10, yields a χ^2 of 46 for 45 degrees of freedom. While this is an acceptable χ^2, the dotted curves do not provide a good description of the P_+ amplitude or relative phase in the region 1.1–1.4 GeV/c^2.

In an attempt to better define the P-wave amplitudes, the D_+ amplitude was fixed to an $f_2(1270)$ Breit–Wigner shape with the amplitude found in the previous fit, and the PWA was redone. The P_+ amplitude and the P_+–D_+ relative phase were fitted as before; Table 2, "Fit B", and Fig. 11 show the result. This fit yields a mass and width for the new resonance, the $\rho(1300)$, of (1290^{+20}_{-30})MeV/c^2 and (120^{+60}_{-50})MeV/c^2, respectively. The resulting description of the data of Figs. 11a and 11b is clearly very good. The dotted curves of Fig. 11 again correspond to no $\rho(1300)$ contribution, and do not provide a good description of the data. Finally, the size of the $\rho(1300)$ amplitude relative to that of the $\rho(770)$ indicates a very small $\pi^+\pi^-$ branching ratio ($\sim$ 4–10%) for this state, assuming the same production mechanism for the two states.

Table 2. Results of fits to P_+ and D_+ magnitudes and relative phase. Errors are statistical only. Fit B comes from the PWA with $|D_+|$ fixed.

Parameter	Fit A	Fit B
$\rho(1300)$ Mass (MeV/c^2)	1290 ± 30	1290^{+20}_{-30}
$\rho(1300)$ Width (MeV/c^2)	90^{+40}_{-30}	120^{+60}_{-50}
$\rho(1300)$ Phase (degrees)	80 ± 20	90 ± 30
$\rho(1300)$ Amplitude (rel. to ρ)	0.28 ± 0.04	0.26 ± 0.05
ρ–$f_2(1270)$ Phase (degrees)	12 ± 10	6 ± 11
χ^2/DoF	23/41	9/33

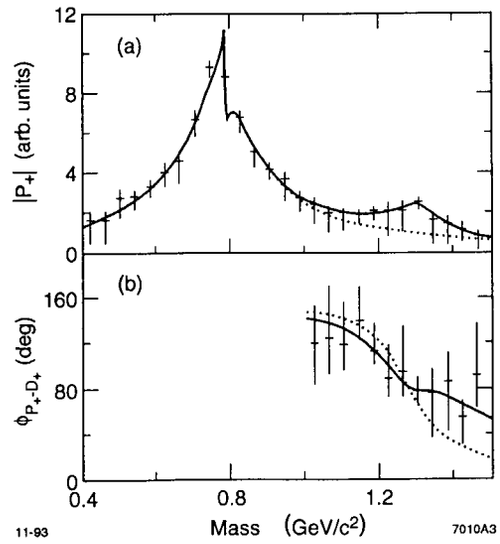

Fig. 11. The mass dependence of (a) the P_+ amplitude and (b) the P_+–D_+ relative phase resulting from the fits to the spherical harmonic moments with the D_+ amplitude fixed. The curves are the same as for Fig. 10.

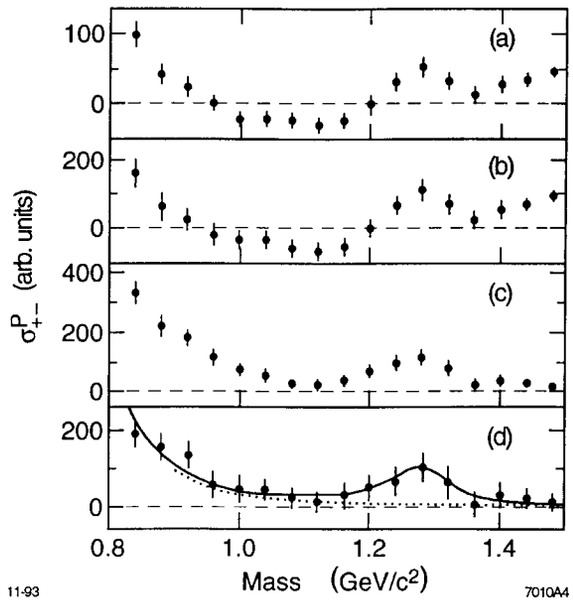

Fig. 12. The σ^P_{+-} projection of the data at different stages of the analysis: (a) the raw data, (b) the acceptance corrected data, (c) the data with the Σ overlap removed, and (d) the data after correction for the overlap cuts. The curve in (d) is the same as for Fig. 11a renormalized to these data.

As further evidence for the $\rho(1300)$, Fig. 12 shows the progression of the quantity σ^P_{+-} through the different stages of the analysis, where σ^P_{+-} is defined as

$$\begin{aligned} \sigma^P_{+-} &\equiv \sqrt{\frac{5}{2}}t_{42} - \sqrt{\frac{10}{3}}t_{22} \\ &= |P_+|^2 - |P_-|^2 \quad \text{(neglecting F-wave)} \end{aligned} \tag{9}$$

and thus results only from P-wave amplitude contributions. The bump in the P-wave around $1.29\,\mathrm{GeV/c^2}$ is clearly visible in all cases, indicating that it is a feature of the data and not an artifact of the analysis. A curve corresponding to the resonance parameters of "Fit B" of Table 2 is drawn on Fig. 12d to show the agreement.

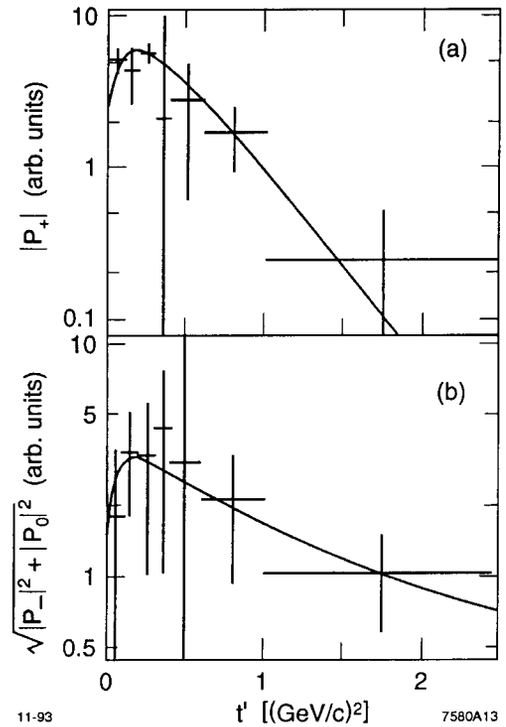

Fig. 13. The (a) P_+ and (b) P-wave unnatural parity exchange amplitudes ($\sqrt{|P_-|^2 + |P_0|^2}$) for the region $1.2 < m_{\pi^+\pi^-} < 1.4\,\mathrm{GeV/c^2}$. The curves show the fits with the exchange mass fixed, as described in the text.

The P- and D-wave t' distributions in the $f_2(1270)$ region were determined by performing a partial wave analysis on the data with $1.2 < m_{\pi^+\pi^-} < 1.4\,\mathrm{GeV/c^2}$. The P_+ and P-wave unnatural parity exchange amplitudes (*i.e.* $\sqrt{|P_-|^2 + |P_0|^2}$) are shown in Fig. 13, while Fig. 14 shows the corresponding D-wave spectra. No correction has been made for the effect of the ρ tail in this region. Following the procedure described above for the ρ differential cross section, the data were fitted with Eqn. (7) with the exchange particle mass free and fixed. Table 3 shows the results.

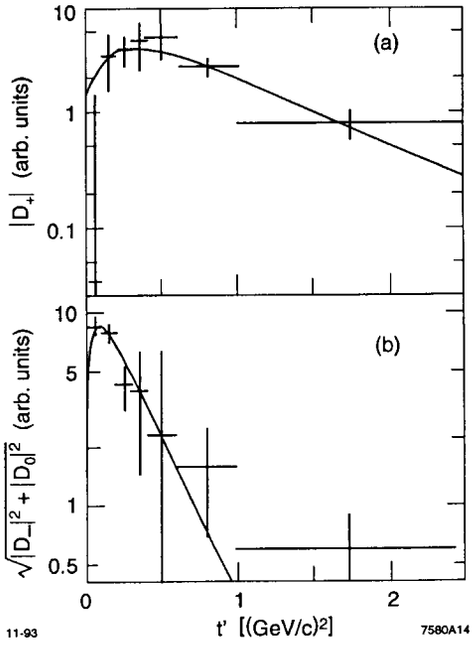

Fig. 14. The (a) D_+ and (b) D-wave unnatural parity exchange amplitudes ($\sqrt{|D_-|^2 + |D_0|^2}$) for the region $1.2 < m_{\pi^+\pi^-} < 1.4\,\mathrm{GeV/c^2}$. The curves show the fits with the exchange mass fixed, as described in the text.

Table 3. The results of fits to the t' spectra for the region $1.2 < m_{\pi^+\pi^-} < 1.4\,\mathrm{GeV/c^2}$.

Quantity	Exchange Mass m_{ex} (MeV/c²)	Slope α ((GeV/c)$^{-2}$)	χ^2/DoF
$\lvert P_+\rvert$	600 ± 200	1.7 ± 1.0	1.0 / 4
	890 (fixed)	2.8 ± 0.7	1.6 / 5
$\sqrt{\lvert P_-\rvert^2 + \lvert P_0\rvert^2}$	690 ± 520	0.6 ± 1.2	0.2 / 4
	493 (fixed)	0.1 ± 0.4	0.5 / 5
$\lvert D_+\rvert$	2130 ± 3610	2.0 ± 1.1	2.2 / 4
	890 (fixed)	1.1 ± 0.3	2.8 / 5
$\sqrt{\lvert D_-\rvert^2 + \lvert D_0\rvert^2}$	330 ± 50	0.7 ± 0.5	2.0 / 5
	493 (fixed)	3.0 ± 1.3	6.1 / 5

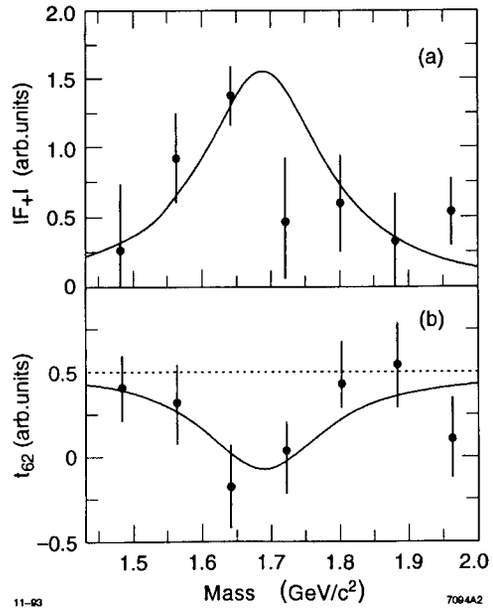

Fig. 15. The mass dependence of (a) the F_+ amplitude and (b) the t_{62} moment from $1.5\,\mathrm{GeV/c^2}$ to $2.0\,\mathrm{GeV/c^2}$ in $80\,\mathrm{MeV/c^2}$ bins. The curves represent a spin 3 Breit–Wigner with the parameters of the $\rho_3(1690)$. Fig. (b) includes a constant background shown as the dotted curve.

5 Analysis of the High Mass Region

In order to determine the wave content of the broad bump in the mass spectrum around $1.7\,\mathrm{GeV/c^2}$, an amplitude analysis allowing up to F-waves was performed in the region 1.5 to $2.0\,\mathrm{GeV/c^2}$ using $80\,\mathrm{MeV/c^2}$ bins. All amplitudes are poorly defined, but there is some evidence for an F-wave resonance around $1.7\,\mathrm{GeV/c^2}$. The amplitude analysis is hampered by residual backgrounds from the Σ overlap that cannot be removed without creating instabilities in the subsequent correction. Fig. 15a shows the F_+ amplitude and Fig. 15b the t_{62} moment, which is proportional to $(|F_+|^2 - |F_-|^2)$. The curves in Fig. 15 are spin 3 Breit–Wigner shapes (Eqns. (5) and (6)) with the mass and width of the $\rho_3(1690)$ (*i.e.* $1690\,\mathrm{MeV/c^2}$ and $215\,\mathrm{MeV/c^2}$ [14]), normalized to the data; the t_{62} curve includes a constant background. The curves are in reasonable agreement with the data, but lack of statistics prevents a definite conclusion.

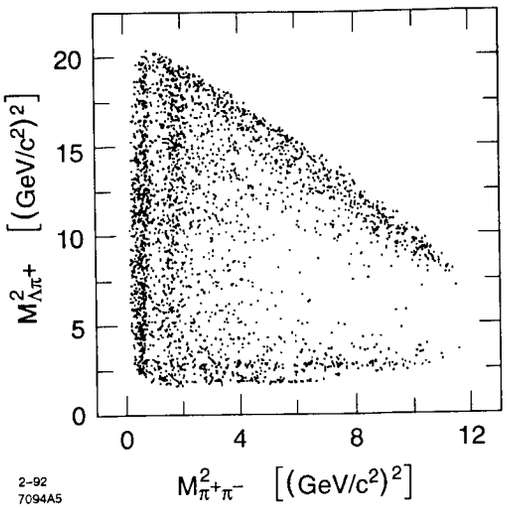

Fig. 16. The Dalitz plot for backward $\pi^+\pi^-$ events ($-t_{K^-\to\Lambda} < 2.0\,(\mathrm{GeV/c})^2$).

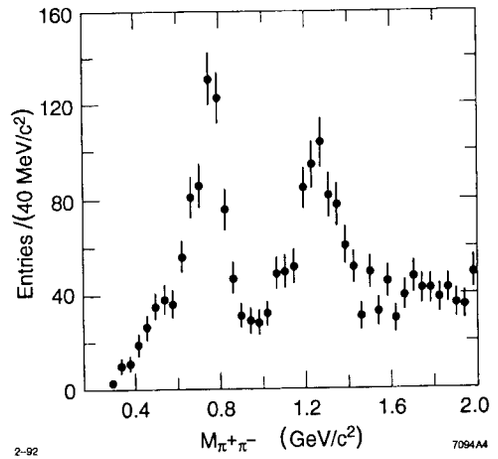

Fig. 17. The mass projection for backward $\pi^+\pi^-$ events.

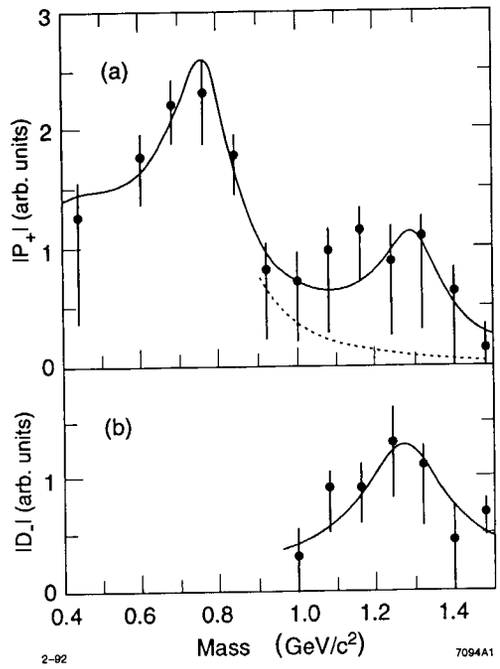

Fig. 18. The mass dependence of (a) the P_+ and (b) the D_- amplitudes for backward $\pi^+\pi^-$. The curves represent a Breit–Wigner fit. The P_+ shape included a factor of (mass)$^{-2}$. The parameters of the resonances, except for the ρ–$\rho(1300)$ phase, were fixed to the values of "Fit B" in Table 2.

6 The Backward $\pi^+\pi^-$ System

Fig. 16 shows the Dalitz plot for the backward $\pi^+\pi^-$ system ($-t_{K^-\to\Lambda} < 2\,(\mathrm{GeV/c})^2$). There are clear bands in the $\pi^+\pi^-$ system at the ρ and $f_2(1270)$. There is also evidence of $\Sigma^+(1385)$ and $\Sigma^-(1385)$ production, as well as the higher mass Σ's seen in the forward data. The $\pi^+\pi^-$ spectrum corresponding to Fig. 16 is shown in Fig. 17, in 80 MeV/c^2 bins. The mass bump around 1.27 GeV/c^2 is stronger relative to the ρ than in the forward $\pi^+\pi^-$ system. There is no clear evidence for any ρ–ω interference effect.

The $\Sigma^+(1385)$ and $\Sigma^-(1385)$ resonances ($m_{\Lambda\pi^\pm} < 1.48\,\mathrm{GeV/c^2}$) were cut out and the moments were corrected for the loss of $\pi^+\pi^-$ events. An amplitude analysis was performed including up to P-wave below 1 GeV/c^2 and up to D-wave from 1 GeV/c^2 to 1.5 GeV/c^2. Figs. 18a and 18b show the mass dependence of the P_+ and D_- amplitudes, respectively;

Table 4. Cross sections for resonances in reaction (1) to decay to $\pi^+\pi^-$. Uncertainties are statistical only, except on the forward $\rho(1300)$ cross section.

Resonance	Cross Section (μb)
Forward ρ	4.74 ± 0.20
Natural parity	3.22 ± 0.12
Unnatural parity	1.57 ± 0.15
Backward ρ	0.21 ± 0.02
Natural parity	0.14 ± 0.01
Total ρ	4.95 ± 0.20
Forward $\rho(1300)$	$0.26 \pm 0.05 \pm 0.06$
Natural parity	0.14 ± 0.04
Forward $f_2(1270)$	1.50 ± 0.14
Natural parity	0.72 ± 0.10
Unnatural parity	0.85 ± 0.11

the D_+ amplitude is relatively small. The curves are Breit–Wigner fits to the amplitudes (Eqn. (8)). The P_+ amplitude function includes a factor of $m_{\pi\pi}^{-2}$, which is necessary to fit the low side of the ρ. This factor was determined empirically from the data, but could be due to the fact that the production mechanism is probably virtual $\overline{\mathrm{p}}\mathrm{p}$ annihilation, which would imply a strong inverse $m_{\pi\pi}$ dependence for the cross section. The $\rho(1300)$ mass and width are fixed to the values of "Fit B" of Table 2, while the masses and width of the ρ and $f_2(1270)$ are fixed to the PDG values [14]. The dotted curve in Fig. 18a is the fit with no $\rho(1300)$ contribution. The fit does support the presence of the $\rho(1300)$ with the same resonance parameters as found in the forward data, but the statistics are very poor.

7 Cross Sections

The cross sections for the production of various resonances produced in reaction (1) were calculated from the fits to the Breit-Wigner shapes. The normalization was determined by integrating the shape for $\pm 5\Gamma_0$ about the resonance mass (the integral was cut off at threshold if necessary). For all resonances, the barrier factor, R, was fixed to $5\,\mathrm{GeV}^{-1}$.

Table 4 lists the resonance cross sections for decay to $\pi^+\pi^-$. The values have been corrected for the visibility of the Λ, using a branching fraction of $(64.1 \pm 0.5)\%$ [14]. The overall normalization of the experiment is $4.095(\mathrm{nb})^{-1} \pm 2.7\%$. Except for the forward total $\rho(1300)$ cross section, the uncertainties listed are statistical only, but include the normalization uncertainty. The ρ cross sections come from fits of the number of events and of the σ^P moments combinations. A linear background was included to allow for the S wave. The $\rho(1300)$ and $f_2(1270)$ cross sections were calculated from the PWA fits. The forward $\rho(1300)$ cross section comes from a fit of the total spin 1 intensity (*i.e.* $|P_+|^2 + |P_-|^2 + |P_0|^2$). However, because

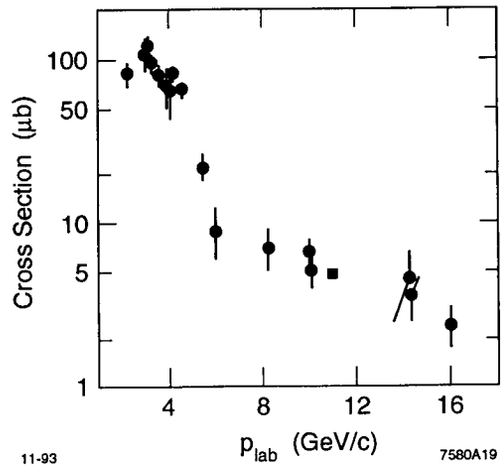

Fig. 19. The total ρ cross section versus laboratory momentum. The current experiment is shown as the solid square; the uncertainty is smaller than the point.

of multiple solutions from the PWA, the intensity is essentially double-valued; therefore, a systematic uncertainty of $0.06\,\mu$b has been added.

Fig. 19 shows the total ρ cross section for many experiments at various laboratory momenta [15]; the current result agrees well with previous experiments. Using the accepted branching fraction for $f_2(1270) \to \pi\pi$ of $0.849^{+0.025}_{-0.013}$ [14] and a Clebsch–Gordan coefficient of 2/3 for the charged mode, a total cross section for forward $f_2(1270)$ of $(2.65 \pm 0.26)\mu$b is obtained.

8 Discussion

In the only other large statistics analysis of the $\pi^+\pi^-$ system in reaction (1) [5], no amplitude analysis was attempted because of the much more severe kinematic overlap with Σ production at the 4.2 GeV/c incident K^- momentum; it was simply assumed that the bump at $\sim 1.27\,\mathrm{GeV/c^2}$ was entirely due to $f_2(1270)$ production. However, measurements of the pion form factor [17] have shown the need for a P-wave resonance with a mass of $\sim 1290\,\mathrm{MeV/c^2}$ and width $\sim 200\,\mathrm{MeV/c^2}$. Also, the P-wave amplitude structure obtained for $\pi^+\pi^-$ elastic scattering in the reaction $\pi^-\mathrm{p} \to \pi^+\pi^-\mathrm{n}$ [16] does show some intriguing irregularity in this mass range. The value of the absorption parameter, η, is systematically below 1 throughout this region by an amount quite consistent with the presence of a ρ state of elasticity of 5–10%. Indeed, the parametrization in Hyams *et al.* of the P-wave amplitude in terms of the ρ and the $\rho(1590)$ (elasticity $\sim 25\,\%$) provides a poor description of the mass dependence of

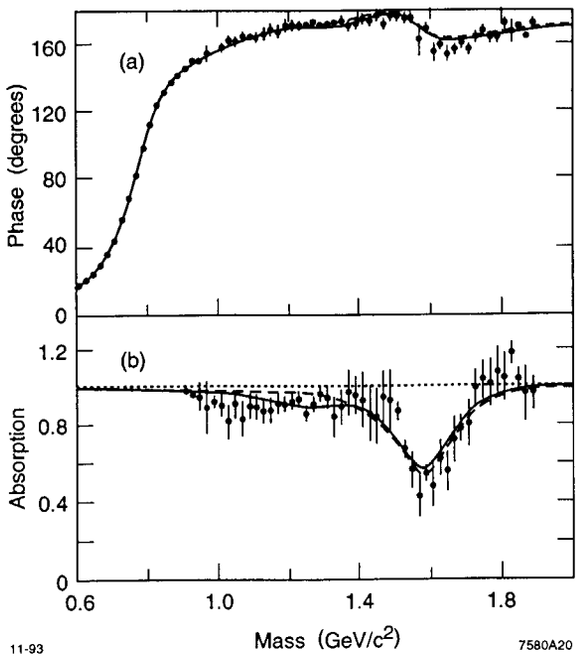

Fig. 20. The P-wave phase shift and absorption from $\pi\pi$ scattering [16]. The dashed curves show the fit with the $\rho(1590)$ and ρ. The solid curves include the $\rho(1300)$ with a width of $200\,\mathrm{MeV/c^2}$.

η, and also of the Y_1^0 and Y_3^0 spherical harmonic moments, in this mass range; the addition of the $\rho(1300)$ with elasticity 5% improves the fit to the η mass dependence (see Fig. 20).

In the context of the $q\bar{q}$ level scheme, the $\rho(1300)$ is most naturally interpreted as the first radial excitation of the ρ. Taken together with the $\rho(1590)$ of Hyams *et al.*, this results in a level structure for the 1^- states in the isovector sector which is remarkably similar to that observed in the strange meson sector [18]. The mass splittings are almost identical, and the first radial excitation has elasticity ~ 5–$10\,\%$ in both cases. In this regard, it should be noted that the rest frame decay momenta for the $\rho(1300)$ and the $K_1^*(1410)$ are almost the same, so that if the small elasticity is related to the nodal structure of the final state radial wave function [19], it would be expected that *both* states should be highly inelastic.

This picture of the isovector 1^- level structure agrees to some extent with that of Donnachie and Mirzaie [20], in that there are indeed two excited ρ states, and each has width $\sim 200\,\mathrm{MeV/c^2}$. Furthermore, the elasticity of the lower mass state is $\sim 5\%$, while that of the higher mass state is $\sim 20\%$ in each case. However, the mass values obtained by Hyams *et al.*

and the present analysis are very different from the $\sim 1.47\,\mathrm{GeV/c^2}$ and $\sim 1.7\,\mathrm{GeV/c^2}$ obtained by Donnachie and Mirzaie. Part of the difference arises from the treatment of the phase of the lower mass excited ρ. This analysis allows the phase to vary; Donnachie and Mirzaie fixed it at 180 degrees, which is in disagreement with the present analysis. Also, it should be pointed out that the model of Donnachie and Mirzaie does not reproduce the mass dependence of the P-wave η parameter in the $1300\,\mathrm{MeV/c^2}$ region as measured by Hyams *et al.*

More recently, Donnachie *et al.* [21] have suggested that the $\rho(1300)$ (referred to as ρ_x by them) does not fit in the isovector multiplet, but rather is a 4-quark $q\bar{q}q\bar{q}$ state. This would suggest that the differential cross section for the $\rho(1300)$ should be steeper than that of a $q\bar{q}$ state since a 4-quark state presumably is a more extended object. However, the exponential slope of the $\rho(1300)$ P_+ amplitude is flatter than that of the ρ, although the difference is only 1.5–2.0 standard deviations. The $\rho(1300)$ unnatural parity exchange amplitude is somewhat flatter than corresponding ρ amplitudes, but the signal is very small, with large uncertainties. Also, while the $f_2(1270)$ is still considered a $q\bar{q}$ state, the slope of the D_+ amplitude is significantly flatter than that of the ρ P_+ amplitude. Therefore, while the present analysis cannot rule out the $\rho(1300)$ being a 4-quark state, the data tend to favor a flatter differential cross section, and therefore a normal $q\bar{q}$ state.

In summary, the $\pi^+\pi^-$ system in reaction (1) has been analysed and has shown a rather striking corroboration of the phenomenon of ρ–ω interference. The measured resonance parameters of the ρ are consistent with the current Particle Data Group values [14], while the differential cross section is consistent with those measured at 4.2 GeV/c [4]. Partial wave amplitude analyses of the forward and backward $\pi^+\pi^-$ data have provided evidence for the existence of a new P-wave state, the $\rho(1300)$, and for the $\rho_3(1690)$. The $\rho(1300)$ is most readily understood as the first radial excitation of the ρ. Its mass and width were found to be $(1290^{+20}_{-30})\mathrm{MeV/c^2}$ and $(120^{+60}_{-50})\mathrm{MeV/c^2}$, respectively. The cross section for forward production was measured as $(0.26 \pm 0.05 \pm 0.06)\mu\mathrm{b}$, implying that the elasticity is small ($\sim$ 4–10%).

References

[1] P. E. Rensing: PhD Thesis SLAC-421 (1993)

[2] D. Aston *et al.*: SLAC-298 (1986); D. Aston *et al.*: Nucl. Phys. **B301** (1988) 525

[3] S. O. Holmgren *et al.*: Phys. Lett. **B66** (1977) 191

[4] M. J. Losty *et al.*: Nucl. Phys. **B133** (1978) 38

[5] M. Aguilar-Benitez *et al.*: Z. Phys. **C8** (1981) 313

[6] M. Baubillier *et al.*: Z. Phys. **C23** (1984) 213

[7] S. N. Ganguli *et al.*: Nuovo Cim. **44A** (1978) 345

[8] A. Martin *et al.*: Nucl. Phys. **B140** (1978) 158; G. Costa *et al.*: Nucl. Phys. **B175** (1980) 402

[9] S. L. Glashow: Phys. Rev. Lett. **7** (1961) 469

[10] S. Coleman, S. L. Glashow: Phys. Rev. **B134** (1964) 671

[11] S. Coleman *et al.*: Proceedings of the XII International Conference on High Energy Physics, Dubna, 1964, Vol. 1. Moscow: Atomizdat (1966) 785

[12] R. Gatto: Nuovo Cim. **28** (1963) 658

[13] J. M. Blatt, V. F. Weisskopf: Theoretical Nuclear Physics. New York: John Wiley & Sons (1952) 361

[14] Review of Particle Properties: Phys. Rev. **D45** (1992)

[15] V. Flaminio *et al.*: Compilation of Cross-sections II: K^+ and K^- Induced Reactions. CERN–HERA 83–02 (1983) 192

[16] B. Hyams *et al.*: Nucl. Phys. **B64** (1973) 134

[17] L. M. Barkov *et al.*: Nucl. Phys. **B256** (1985) 365

[18] W. Dunwoodie: Proceedings of the Rheinfels Workshop on the Hadron Spectrum, St. Goar, Germany, September 3–6, 1990. Amsterdam: North Holland (1991) 16

[19] A. Bradley: J. Phys. **G4** (1978) 1517; A. le Yaouanc *et al.*: Phys. Lett. **B76** (1978) 484; E. Eichten *et al.*: Phys. Rev. **D21** (1980) 203; S. B. Gerasimov, A. B. Govorkov: Z. Phys. **C13** (1982) 43

[20] A. Donnachie, H. Mirzaie: Z. Phys. **C33** (1987) 407

[21] A. Donnachie, Yu. S. Kalashnikova: Z. Phys. **C59** (1993) 621; A. Donnachie, Yu. S. Kalashnikova, A. B. Clegg: Z. Phys. **C60** (1993) 187